



Quarterly Report #4

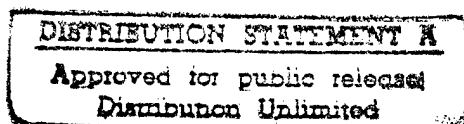
The Reliability of Laser Reflowed Sn-Ag Solder Joints

C.H. Raeder, D.L. Millard, and R.W. Messler

Center for Integrated Electronics and Electronics Manufacturing, (formerly the Design and Manufacturing Institute) Rensselaer Polytechnic Institute, Troy, NY 12180

4.1 Literature Review of Experimental Thermomechanical Hysteresis Measurement

Measurement of thermal cycling stress-strain hysteresis for soldered joints is described by several authors [1-5]. In the first study to report experimentally measured thermomechanical (T-M) stress-strain hysteresis [1,2], only a single ceramic leadless chip carrier soldered to a fiberglass reinforced polymer (FR4) printed wiring board and a single thermal cycle was used throughout the study. These conditions prescribe one value of k' and one value of γ_{fc} . Only stable loop hysteresis was reported. The results were thus very limited. Y.-H. Pao [3,4] used a 2-beam, model geometry very similar to that of Figure 3.1 and a single temperature cycle to successfully measure the T-M hysteresis of a variety of Sn-based alloys. The stress-strain data were used to obtain constitutive relations describing the time, temperature and stress dependent deformation behavior of the test alloys under thermal cycling conditions. These data may be applicable to other combinations of γ_{fc} and k' , but the influence of γ_{fc} and k' , on T-M fatigue lifetime remains unaddressed. Haacke, Sprecher, and Conrad [5] briefly describe a thermomechanical test assembly which is composed of a load frame, insert and solder joint prepared separately.



19951026 089



OFFICE OF THE UNDER SECRETARY OF DEFENSE (ACQUISITION)
DEFENSE TECHNICAL INFORMATION CENTER
CAMERON STATION
ALEXANDRIA, VIRGINIA 22304-6145

IN REPLY
REFER TO

DTIC-OCC

SUBJECT: Distribution Statements on Technical Documents

TO: OFFICE OF NAVAL RESEARCH
CORPORATE PROGRAMS DIVISION
ONR 353
800 NORTH QUINCY STREET
ARLINGTON, VA 22217-5660

1. Reference: DoD Directive 5230.24, Distribution Statements on Technical Documents, 18 Mar 87.

2. The Defense Technical Information Center received the enclosed report (referenced below) which is not marked in accordance with the above reference.

QUARTERLY REPORT #4
N00014-93-1-1295
TITLE: THE RELIABILITY OF LASER
REFLOWED Sn-Ag SOLDER JOINTS

3. We request the appropriate distribution statement be assigned and the report returned to DTIC within 5 working days.

4. Approved distribution statements are listed on the reverse of this letter. If you have any questions regarding these statements, call DTIC's Cataloging Branch, (703) 274-6837.

FOR THE ADMINISTRATOR:

1 Encl

GOPALAKRISHNAN NAIR
Chief, Cataloging Branch

FL-171
Jul 93

1995 1026 089
680 0701 5661

DISTRIBUTION STATEMENT A:

APPROVED FOR PUBLIC RELEASE: DISTRIBUTION IS UNLIMITED

DISTRIBUTION STATEMENT B:

DISTRIBUTION AUTHORIZED TO U.S. GOVERNMENT AGENCIES ONLY;
(Indicate Reason and Date Below). OTHER REQUESTS FOR THIS DOCUMENT SHALL BE REFERRED
TO (Indicate Controlling DoD Office Below).

DISTRIBUTION STATEMENT C:

DISTRIBUTION AUTHORIZED TO U.S. GOVERNMENT AGENCIES AND THEIR CONTRACTORS;
(Indicate Reason and Date Below). OTHER REQUESTS FOR THIS DOCUMENT SHALL BE REFERRED
TO (Indicate Controlling DoD Office Below).

DISTRIBUTION STATEMENT D:

DISTRIBUTION AUTHORIZED TO DOD AND U.S. DOD CONTRACTORS ONLY; (Indicate Reason
and Date Below). OTHER REQUESTS SHALL BE REFERRED TO (Indicate Controlling DoD Office Below).

DISTRIBUTION STATEMENT E:

DISTRIBUTION AUTHORIZED TO DOD COMPONENTS ONLY; (Indicate Reason and Date Below).
OTHER REQUESTS SHALL BE REFERRED TO (Indicate Controlling DoD Office Below).

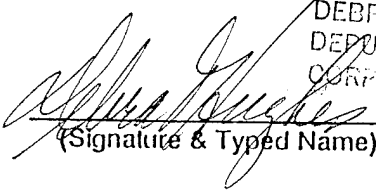
DISTRIBUTION STATEMENT F:

FURTHER DISSEMINATION ONLY AS DIRECTED BY (Indicate Controlling DoD Office and Date
Below) or HIGHER DOD AUTHORITY.

DISTRIBUTION STATEMENT X:

DISTRIBUTION AUTHORIZED TO U.S. GOVERNMENT AGENCIES AND PRIVATE INDIVIDUALS
OR ENTERPRISES ELIGIBLE TO OBTAIN EXPORT-CONTROLLED TECHNICAL DATA IN ACCORDANCE
WITH DOD DIRECTIVE 5230.25, WITHHOLDING OF UNCLASSIFIED TECHNICAL DATA FROM PUBLIC
DISCLOSURE, 6 Nov 1984 (Indicate date of determination). CONTROLLING DOD OFFICE IS (Indicate
Controlling DoD Office).

The cited documents has been reviewed by competent authority and the following distribution statement is
hereby authorized.

<p><u> A </u> (Statement)</p>	<p>OFFICE OF NAVAL RESEARCH CORPORATE PROGRAMS DIVISION ONR 353 800 NORTH QUINCY STREET ARLINGTON, VA 22217-5660</p>	<p>_____ (Controlling DoD Office Name)</p>
<p>_____ (Reason)</p>	<p>DEBRA T. HUGHES DEPUTY DIRECTOR CORPORATE PROGRAMS OFFICE</p>	<p>_____ (Controlling DoD Office Address, City, State, Zip)</p>
<p><u></u> (Signature & Typed Name)</p>	<p>_____ (Assigning Office)</p>	<p>19 SEP 1995 _____ (Date Statement Assigned)</p>

Characterization of the test assembly in [5] is incomplete so the thermomechanical fatigue results reported are difficult to interpret.

Experimental test assembly and solder joint configurations vary, but the approaches are, in theory, similar. The general approach is shown in Figure 3.1. If strain gages are attached to the top and bottom of either the component, substrate, or one of the beams representing these package elements in a model assembly, bending and elongation of the component or beam can be recorded. Bending in the other beam is either measured in the same way or assumed equal to that of the first beam. Stress in the solder joint is calculated from the elastic mechanical strain in the beam, Equations 3.3 and 3.4 Strain in the solder joint is calculated from the thermal and mechanical strain in the beams according to Equation 3.10.

Thermal cycling of solder joints to eventual fatigue failure is also reported in the literature [6-12]. These studies report failures as a function of thermal cycles, but only one combination of γ_{fc} and k' is addressed in each study and the value of k' for many test assemblies is not known. One study [13,14] broadly addresses the pertinent variables of γ_{fc} and k' . That study reports TMF failures in Sn-Pb solder joints of actual electronic assemblies which occurred over a long service time and/or temperature cycling period. By using actual electronic assemblies, the results are easily applied but the conditions of stress are complex. The failure process was not addressed in this study. Measurement of stress and strain in solder joints of actual electronic assemblies is impractical if not impossible. In addition, if a variety of alloys are to be tested, separate electronic assemblies must be constructed for each alloy. Cost and time constraints demand a more expeditious experimental approach in qualifying a new solder alloy.

k' and γ_{fc} are the important parameters in any evaluation of thermomechanical fatigue lifetime. A test assembly or minimum number of test assemblies is needed which can address a variety of test conditions efficiently.

<input checked="" type="checkbox"/>
<input type="checkbox"/>
<input type="checkbox"/>

per lti

Availability Codes	
Dist	Avail and/or Special
A-1	

4.2 The Thermomechanical Fatigue Test Assembly

At present, the number and type of electronic components and substrates in use define a practical spectrum of values of γ_{fc} and k' to incorporate into an experimental test program. Leaded components have the lowest values of stiffness, typically on the order of 40MPa [15,16], whereas leadless and discrete components have the highest stiffness, reaching 200-300 MPa. γ_{fc} is equally variable, reaching as high as 25%. A practical minimum limit for experimentation is between 1 and 2%.

The first requirement of an effective test assembly is that one must be able to calculate stress and strain in the solder joint from measurements and physical constants. Stress and strain are basic quantities and this enables the investigator to track the evolution of the hysteresis and detail the deformation behavior as a function of cycling. Also, testing to be interrupted at prescribed conditions for metallurgical examination. The second requirement, of equal importance, is the ability to vary k' and γ_{fc} . Figure 4.1 is a schematic of the test assembly proposed to satisfy these requirements. A similar assembly has been used previously [5], though the stiffness of the load frame was not measured in advance or varied during fatigue testing. For the present study, load frames will be machined to different specifications from a variety of metallic materials to vary stiffness. Specific test conditions are given later.

The load frame is fitted with two strain gages on the top and bottom of the thin, top beams, each located 1/4 of the distance from the side beams to the central joint insert area. The side and bottom beams are thick in comparison to the top beam so most of the deflection which appears in the frame occurs in the top beam. An insert made of a different material than the frame is bolted to the frame through the bottom beam as shown in Figure 4.1. This difference in material between insert and load frame gives rise to the different levels of CTE mismatch.

The solder joint is a butt joint made between two pieces of copper, each prepared separately as described in detail later. The joint assembly is situated so that the joint is

coplanar with the vertical interface between the frame and insert. It is then fixed in place with set screws. The maximum thermal displacement, l_{th} , for a given temperature cycle is set by the thermal expansion mismatch and the distance, L , between the solder joint center and the interface of the insert and the load frame. The frame stiffness, k , can be estimated by beam analysis or is measured by a calibration procedure described in Appendix 1. A separate load frame is required for each desired value of frame stiffness, but, once fitted with strain gages, the frame may be reused for an indefinite number of tests. Different values of γ_{fc} are obtained by using a series of insert materials, as listed later.

Figure 4.2 shows a schematic of the strain gage configuration, temperature sensor, and data acquisition system. A full Wheatstone bridge is used with strain gages mounted on the top and bottom of the top load frame beam as described earlier. A constant 5 volt dc power supply is used for strain gage bridge excitation. The strain gage output is fed to a signal conditioner which amplifies the dc voltage 500x. This signal is fed to a 16 bit, A/D converter card inside a Macintosh IIx. Temperature is read from a T-type thermocouple affixed with thermally-conducting epoxy to the bottom base beam of the load frame. This signal is also fed to a signal conditioner which linearizes and scales the signal between 0 and 5 volts, corresponding to -100 and 400°C, respectively, and then to the Macintosh IIx.

4.3 The Solder Joint

As shown in Figure 4.1, the solder joint being tested is a butt joint between two 1/8" diameter commercially pure Cu rods. The rod ends to be soldered are polished to a flat finish using 600 grit paper and with the aid of an epoxy block drilled to accommodate several of the Cu rods perpendicular to the polishing surface. After polishing, the rods are cut to 3/8" length for the joint. The Cu piece is then coated everywhere except in the joint area with carbon paint (the same conductive paint used in electron microscopy) to serve

as solder resist. Following drying, two Cu pieces with the joint areas coated with flux and separated by a piece of solder alloy of the desired joint thickness and composition are aligned in a solder-resist coated clamping fixture. The Cu pieces, solder spacer, and clamp fixture are immersed in molten solder to form the solder joint. For the present study, an initial joint thickness, h , of 254 μm will be used.

4.4 Experimental Procedure

The load frame calibration procedure is given in Appendix 1. Following calibration of the load frame and solder joint reflow, the joint assembly is aligned in the insert and the set screw of the insert is tightened to 3 N·m. The insert and joint are then aligned in the load frame and are fixed by the bolt in the bottom frame member and a set screw threaded through the top frame member (Figure 4.1). Both fasteners are tightened to 3 N·m.

The thermal cycle chosen for the present study is a 66 min. cycle between -15°C and 125°C , including 8 min. hold times at the temperature extrema (the temperature cycle is shown in Figure A3). This temperature cycle was chosen because no military specification exceeds the 125°C limit and the maximum temperature ramp rate of the Cincinnati Sub Zero thermal chamber used becomes increasingly slower at temperatures below -15°C .

4.5 Experimental Thermomechanical Hysteresis

The thermomechanical testing system described above was used to collect stress-strain hysteresis on a solder joint made with eutectic Sn-Ag solder. Figure 4.3 shows the stress-strain response of the solder joint from the start of the experiment to the end of the 2nd thermal cycle, and for the 39th-46th thermal cycles where the hysteresis loop seemed to have stabilized.

At the start of the experiment, the load frame is at room temperature. The starting condition of stress is set with the use of stacked shims which have a minimum dimension of 12.7 μm . These are inserted between the frame and insert (Figure 4.1). The level of pre-set stress is chosen to correspond as closely as possible to the average room temperature stress in the stable hysteresis loop. There are four reasons for choosing this level of pre-set stress: First, the net strain which occurs prior to reaching the stable loop will be at a minimum thereby eliminating one variable present otherwise. Second, a minimum number of cycles are necessary to attain the stable loop. Third, the stable loop occurs nearest to the zero point of strain, which is the as-soldered condition. The desired level of pre-set stress is determined from the numerical simulation of stress-strain hysteresis given in Appendix 2. The load frame test assembly is then inserted in the thermal cycling chamber and testing begins.

In Figure 4.3, the joint is initially under some stress, $\approx 5\text{MPa}$, but the displacement and strain in the solder at this initial stress are assigned a null value. This necessarily implies that $l_{\text{th}} = l_{\text{mech}} \neq 0.0$ at time equal to zero. Note that the starting value of stress in Figure 4.3 was not set as described above, as stable hysteresis did not occur near the starting point. The desired starting point is shown in the figure. At stable hysteresis, the shear strain range in the solder joint is $\approx 1.3\%$ and the stress range is $\approx 23\text{MPa}$.

After reaching the stable hysteresis loop continued thermal cycling causes damage to the solder joint. The stress range decreases and the strain range increases. This will be referred to as post-stable (PS) hysteresis and is shown in Figure 4.4. Complete separation of the solder joint occurred at approximately 250 cycles.

A consistent definition of failure is necessary. The occurrence of failure would most easily be defined by a certain % stress reduction or % strain increase between the failure cycle and the stable cycle or could be defined by some change in plastic strain energy of the hysteresis. These measures, for the example hystereses of Figures 4.3 and

4.4 are plotted vs. thermal cycles in Figure 4.5. The hysteresis is stable from cycles 5-40. Note that for these example hystereses, the test was interrupted once after the 50th cycle. This resulted in premature deviation from the stable loop. The number of stable loops that would have occurred otherwise is not known, but, assuming the number is not tremendously greater than the number of stable loops observed, a significant portion of the life of the solder joint may be spent in crack propagation if it is assumed that stable hysteresis corresponds to crack initiation and that PS cycling corresponds with crack growth. Regardless, after the 50th cycle, the strain range increases and the stress range decreases steadily.

The strain energy per cycle, calculated from the area enclosed by the hysteresis loop, rises after stable cycling, reaches a peak, and then decreases to eventual joint separation. At present, the strain energy maximum will be defined as the failure point because strain energy incorporates both stress and strain, and because the strain energy reaches a peak between the minimum strain energy, which occurs at the stable loop, and complete separation of the solder joint. This criteria may be adjusted later should the need arise.

References

1. P.M. Hall, I.E.E.E. Trans. C.H.M.T., 7 (1984) p. 314.
2. P.M. Hall, I.E.E.E. Trans. C.H.M.T., 12 (1987) p. 556.
3. Y.-H. Pao, S. Badgley, R. Govila, L. Baumgartner, R. Allor, and R. Cooper, J. Elec. Packaging, 114 (1992) p. 135.
4. Y.-H. Pao, S. Badgley, R. Govila and E. Jih, Mat. Res. Soc. Symp. Proc., Vol. 323, 1994, p. 153.
5. P. Haacke, A.F. Sprecher, and H. Conrad, J. Elec. Packaging, 115 (1993) p. 153.
6. L.R. Fox, J.W. Sofia and M.C. Shine, I.E.E.E. Trans. C.H.M.T., 8 (1985) p. 275.
7. M. Harada and R. Satoh, I.E.E.E. Trans. C.H.M.T., 13 (1990) p. 736.
8. S-M Lee, D.S. Stone, I.E.E.E. Trans. C.H.M.T., 14 (1991) p. 628.
9. Y.-H. Pao, R. Govila, S. Badgley and E. Jih, J. Elec. Packaging, 115 (1993) p. 1.
10. E.P. Busso, M. Kitano, and T. Kumazawa, J. Elec. Packaging, 116 (1994) p. 6.
11. R.K. Govila, E. Jih, Y.-H. Pao, and C. Larner, J. Elec. Packaging, 116 (1994) p. 83.
12. J-P. Clech, J.C. Manock, D.M. Noctor, F.E. Bader and J.A. Augis, Proceedings 43rd E.C.T.C., Orlando, FL, June 1-4, 1993, p. 62.
13. J-P. Clech, D.M. Noctor, J.C. Manock, G.W. Lynott, And F.E. Bader, I.E.E.E. Trans. C.H.M.T., 17 (1994) p. 487.
14. R.W. Kotlowitz, and L.R. Taylor, I.E.E.E. Trans. C.H.M.T., 14 (1991) p. 299.
15. L.S. Goldman, J. Elec. Packaging, 116 (1994) p. 23.
16. MIL-HDBK-5F, Metallic Materials and Elements for Aerospace Vehicle Structures, V. 1, 1 Nov. 1990, p. 3-241
17. Y.S. Touloukian, R.K. Firby, R.E. Taylor, and P.D. Desai, Thermophysical Properties of Matter, Vol. 12, Thermal Expansion Metallic Elements and Alloys, Plenum, New York, p. 1113.

18. Structural Alloys Handbook, ed. J.M. Holt, H. Mindlin, and C.Y. Ho, Publ. CINDAS/Purdue Univ., 1293 Potter Engineering Center, Rm. 316B, West Lafayette, IN 47907-1293.
19. C.H. Raeder et. al., Proc. 16th IEEE/CHMT Int. Elec. Man. Tech. Symp., Sept. 12-14, 1994, La Jolla, CA, P. 1.
20. B.M. Drapkin and V.K. Kononenko, Izvetiya Akademii Nauk S.S.S.R. Metally, 2 (1987) 162.
21. J.P. Clech and L.A. Augis, Proc. 7th Int. Elec. Packaging Conf., Boston, MA, Nov. 1987, Vol. 1, p. 385. and Proc. 1988 IEPS, Dallas, Nov. 1988, p. 305.
22. H.J. Frost and M.F. Ashby, Deformation Mechanism Maps, Pergamon Press, Elmsford, New York (1982) pp. 1-7.

Appendix 1. LOAD FRAME CALIBRATION PROCEDURE

A1.1 Calibration for Load

Calibration for load, P , is done with a dead weight hung from the center joint insertion point. This yields a plot of load vs. voltage as a function of temperature as seen in Figure A1.1, obtained here from a brass load frame. During data reduction, a multiple regression fit is used to obtain load at any temperature as a function of voltage. Note that the linear fit of each curve given at the bottom of Figure A1.1 shows that the slope of the load vs. voltage plot changes as a function of temperature. This is due to the combined effects of the decrease in the elastic modulus of the test fixture with increasing temperature and the decrease in gage factor with increasing temperature of the strain gages.

Young's modulus as a function of temperature is given by (Machine Design, 1984):

$$E(T) = E_0 \left(1 - \beta \frac{T - 298}{T_M} \right) \quad (A1.1)$$

where E_0 is Young's modulus at room temperature, β is a constant, T is the test temperature in $^{\circ}\text{K}$, and T_M is the melting temperature in $^{\circ}\text{K}$. The room temperature modulus of yellow brass is 101,000 MPa, $\beta = 0.53$, and $T_M = 1205^{\circ}\text{K}$. The variation of gage factor, g , with temperature is given by the strain gage manufacturer (Micro-Measurements Division, Measurements Group, Inc., gage type WK-13-062AP-350) as:

$$g(T) = 2.09(1 - 0.017(T - 297)) \quad (A1.2)$$

Figure A1.2 shows a plot of the % change in voltage expected due to the temperature variation in E , g , and $E+g$, and the experimentally measured values of dV/dP (obtained from the dead weight calibration) vs. temperature, all normalized about the median

temperature of 55°C. Note that the elastic modulus decreases with temperature, so the expected voltage read from the strain gages for a given load increases with temperature.

There is a very clear correspondence between the experimentally measured normalized values of dV/dP and the calculated temperature dependence of $E+g$. This correspondence is used later to calculate the temperature dependence of load frame stiffness. It is not used when calculating load from the measured voltage, however.

A1.2 Calibration for Mechanical Displacement

Calibration for displacement is done by using the same set of inserts as will be used for actual TMF testing. First, the load frame is subjected to a thermal cycle with no insert, i.e., stress free. The voltage vs. temperature plot is recorded. Second, an insert with a dissimilar thermal expansion coefficient is installed and pinned with a stainless steel pin (as opposed to a copper pin with a solder joint that will be used in TMF testing as shown in Figure 3.5). Similar voltage vs. temperature cycles are recorded for each insert material used.

Figure A1.3 shows the test temperature cycle and representative plots of voltage vs. temperature for the brass load frame with a variety of insert materials. At zero stress, the voltage output is approximately constant, 1.1 V, with changes in temperature. There is no change in slope of the calibration curves as they pass through the zero stress curve, demonstrating that there is no mechanical play or backlash in the system. The calibration curves need not, however, pass through the zero stress curve because each test represents only a single value of displacement, voltage varies linearly with displacement (as shown in the load calibration), and there is no play in the system.

The thermal displacement, Δl_{th} , for the given frame and insert material is calculated from the thermal expansion mismatch. Figure A1.4 shows the thermal expansion data [16-18] and linear equations used to fit the data for all materials used in the study. During displacement calibration, Δl_{sold} is equivalent to the strain in the

stainless steel pin. This is assumed to be negligible, so $\Delta l_{\text{mech}} = \Delta l_{\text{th}}$. The voltage difference measured between the temperature extrema, $\Delta V (=V_{\text{max}} - V_{\text{min}})$, is plotted vs. Δl_{mech} in Figure A1.5 for the brass load frame. The same temperature excursion is used in all displacement calibrations and the gage factor varies linearly with temperature so the value of dl_{mech}/dV obtained applies to the median temperature, 55°C. When calculating strain, dl_{mech} is multiplied by the gage factor normalized around 55°C.

A1.3 Calculation of the Assembly Stiffness, k & k'

The assembly stiffness, k, is given by Equation (3.3). Figure A1.1 is used to obtain $(dP/dV)_{55^\circ\text{C}}$ and Figure A1.5 gives $(dl_{\text{mech}}/dV)_{55^\circ\text{C}}$. The assembly stiffness at the median temperature, k_{55° , is given by $(\Delta P/\Delta V)_{55^\circ} / (\Delta l_{\text{mech}}/\Delta V)_{55^\circ\text{C}}$. The assembly stiffness at any other temperature is calculated by multiplying k_{55° by the load frame modulus normalized around 55°C. The assembly stiffness, both k and k' (for the solder joint geometry used), of the brass rig used as an example throughout this discussion is shown in Figure A1.6 as a function of temperature.

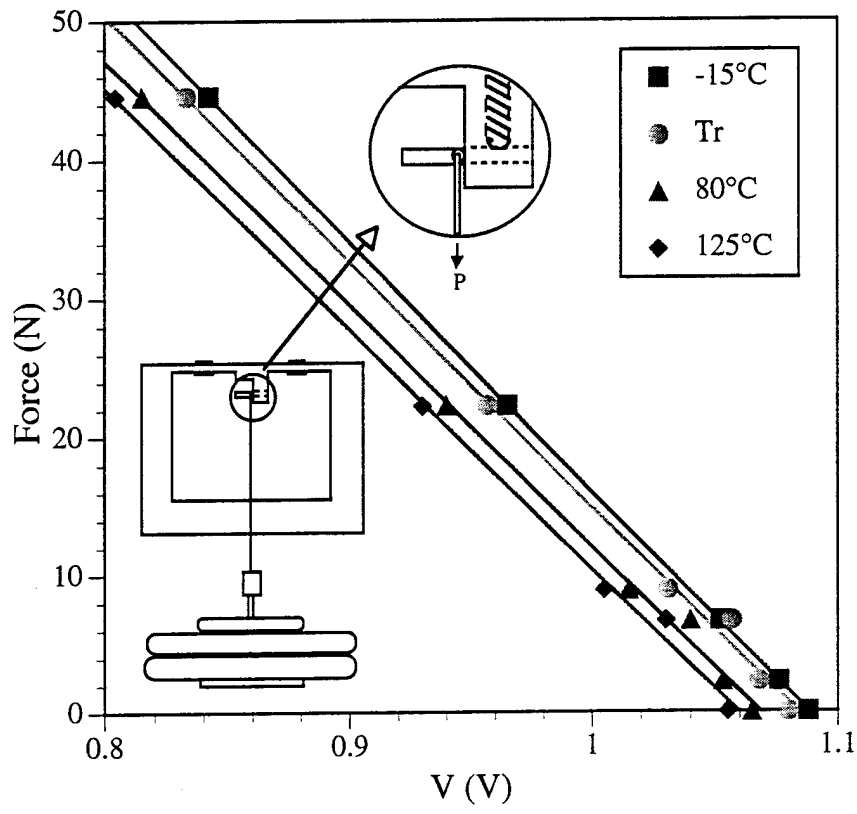


Figure A1.1. Dead weight calibration of load frame.

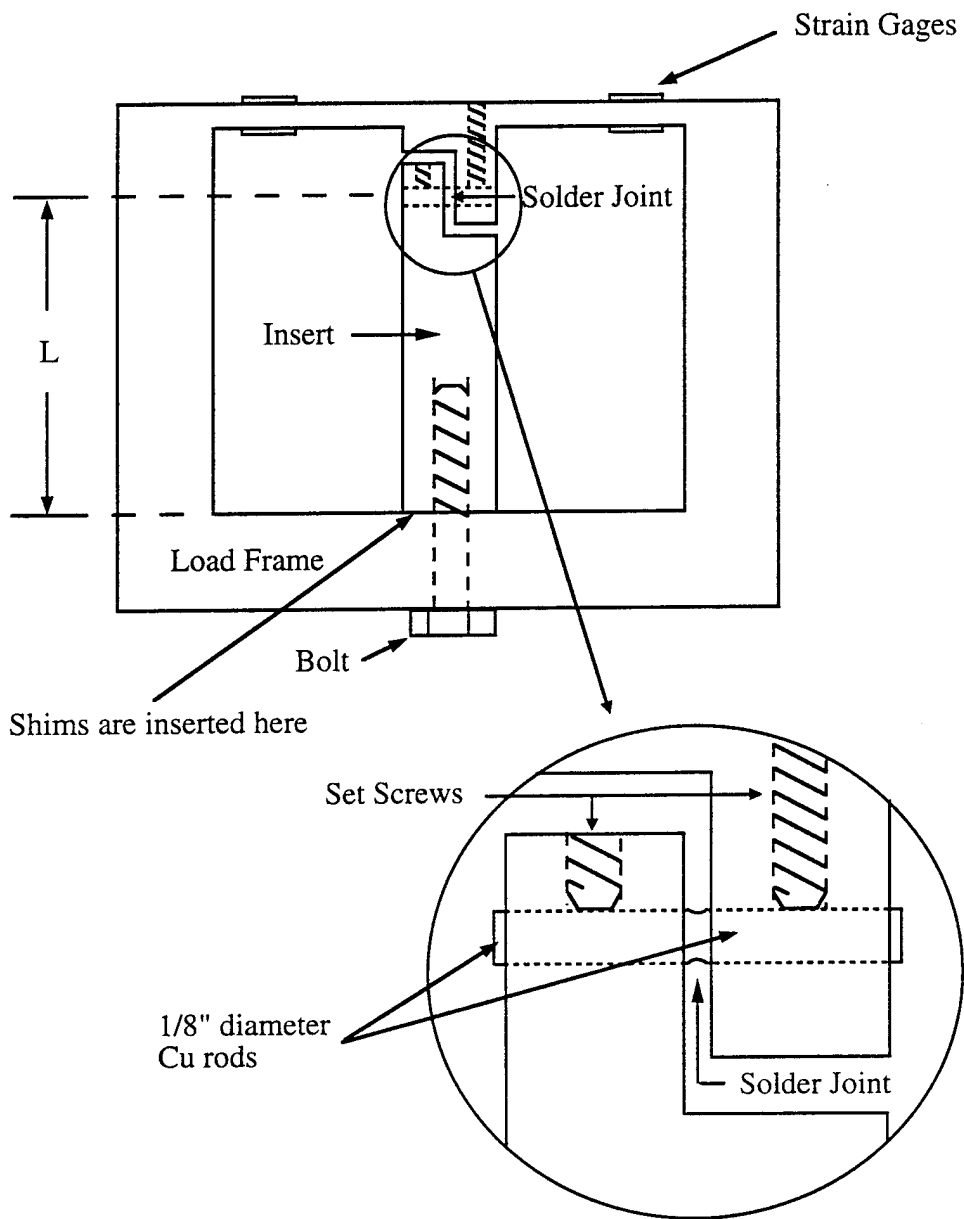


Figure 4.1. Schematic of test assembly: load frame and insert of differing thermal expansion coefficients; stress and strain determined by strain gage measurements.

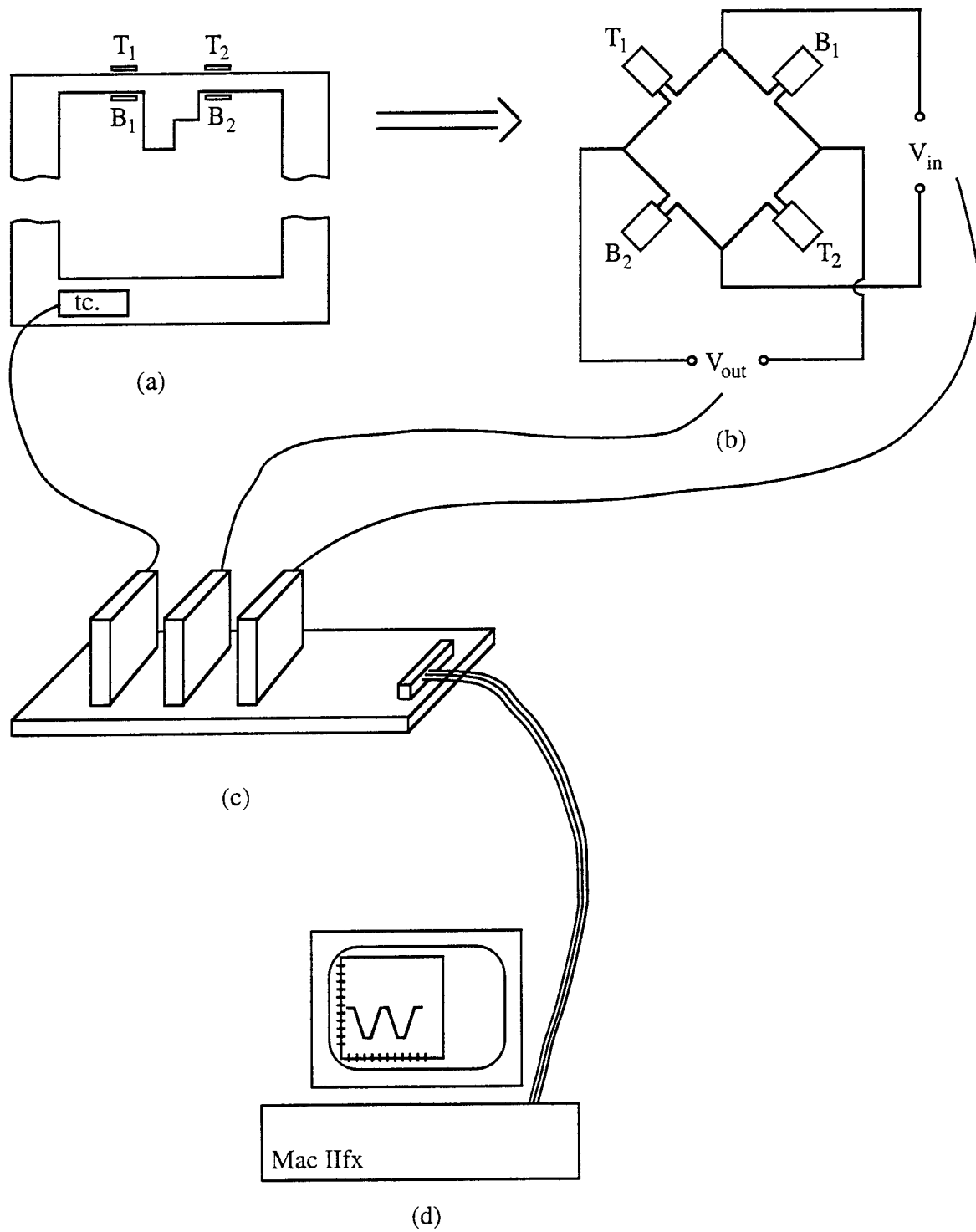


Figure 4.2. Data acquisition system: a) load frame assembly; b) Wheatstone bridge; c) signal conditioners (power supply, 5V, Amplifier, 500x, linearized thermocouple output); d) A/D card and Macintosh computer.

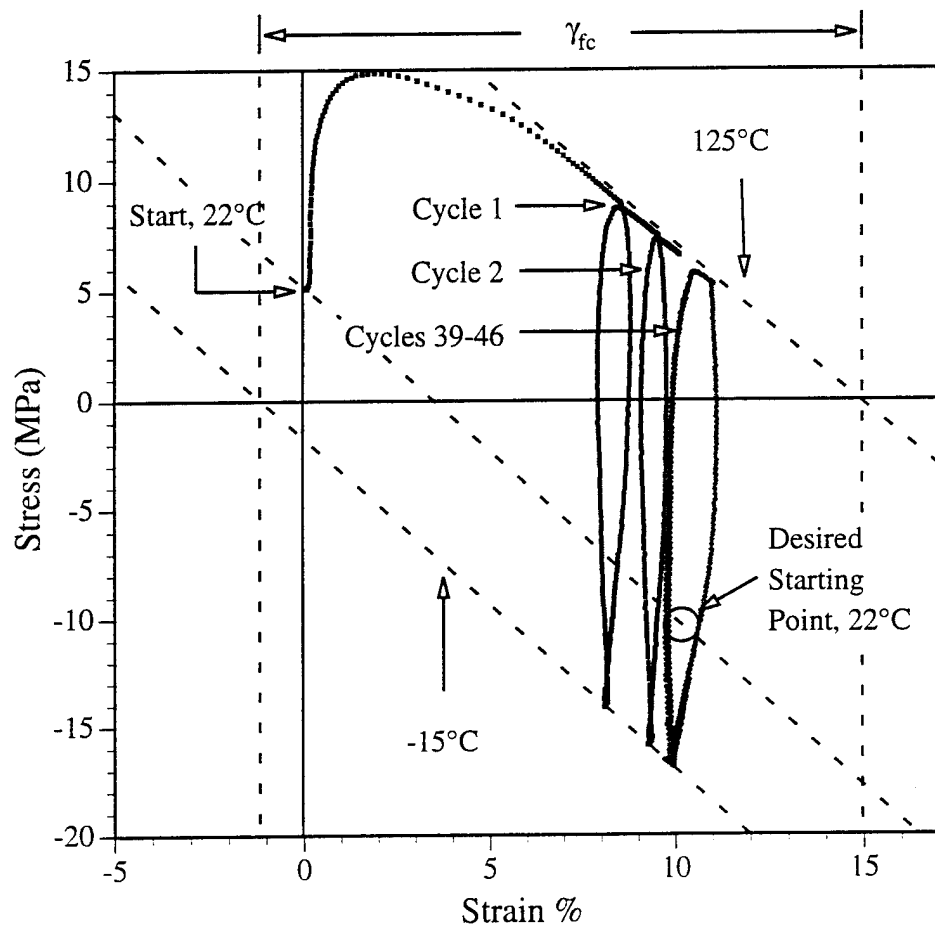


Figure 4.3. Thermomechanical stress-strain hysteresis in an eutectic Sn-Ag solder joint, thermal cycled from -15°C to 125°C in 66 min., with $k' = 150$ MPa, $\gamma_{fc} = 16\%$, cycles 1,2, and 39-46.

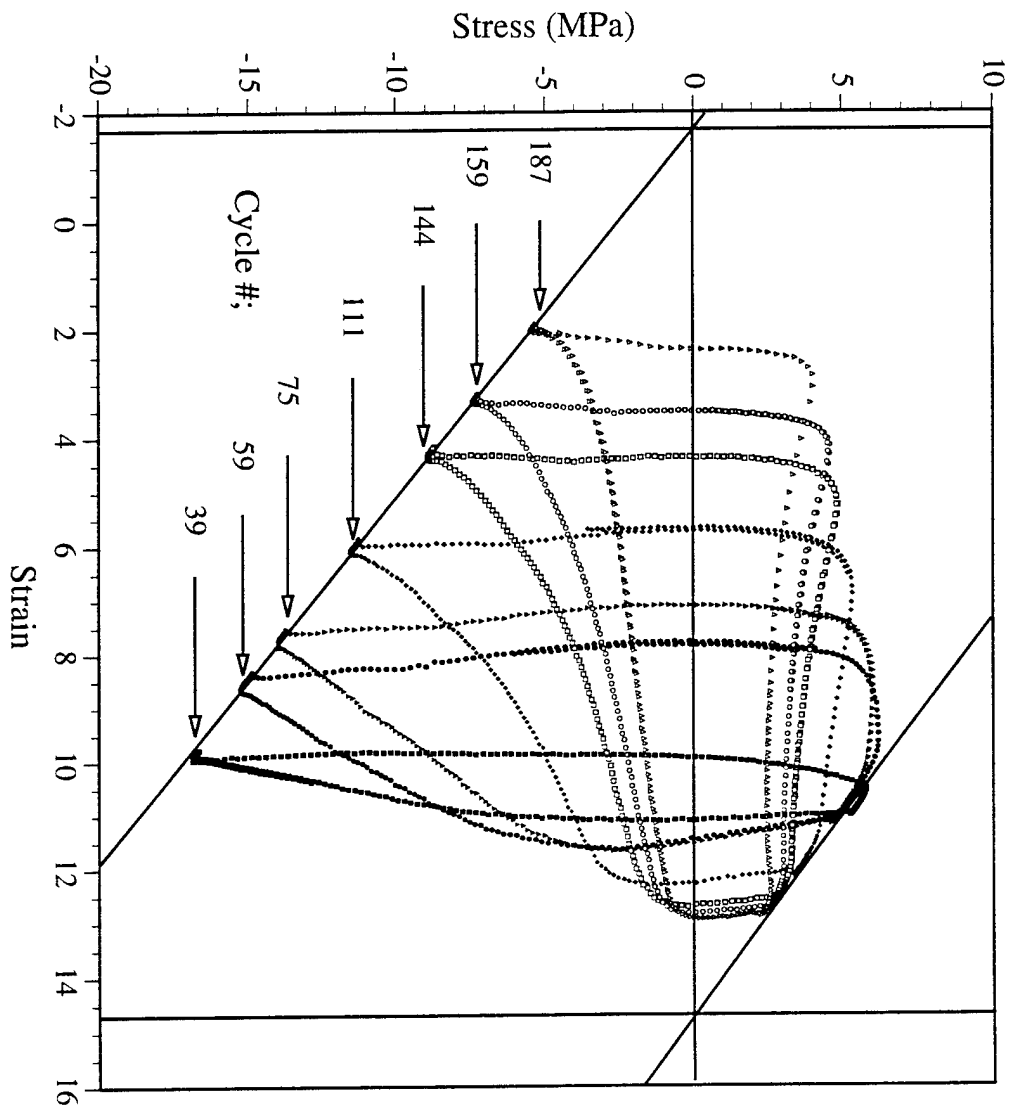


Figure 4.4. Post-stable hysteresis of SnAg solder joint, -15 to 125°C, $k' = 150$ MPa, $\gamma_{fc} = 16\%$.

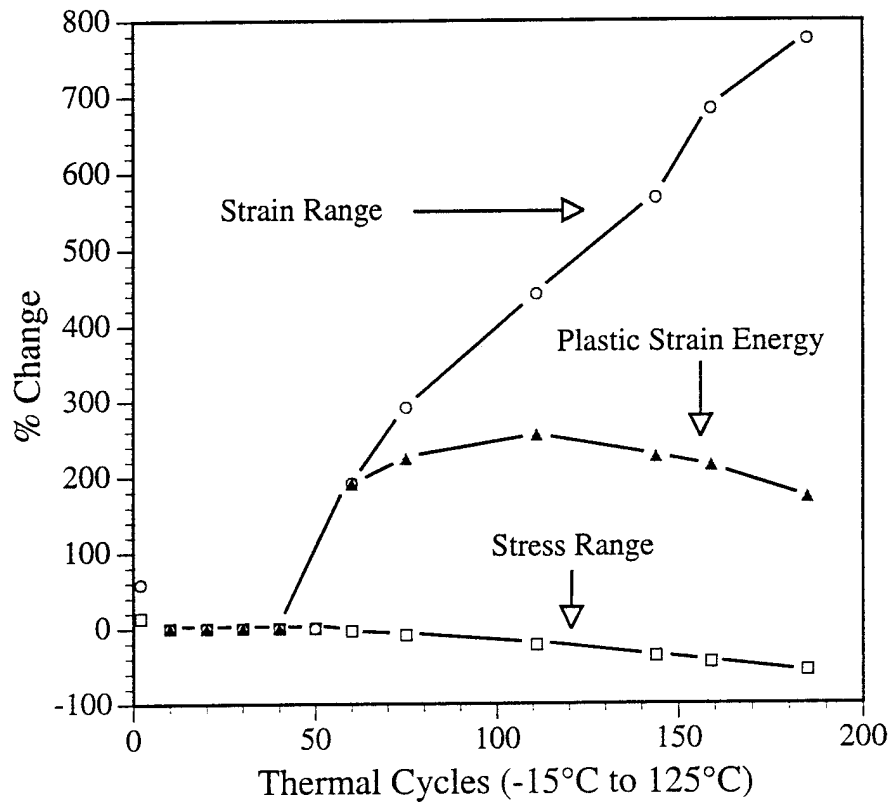


Figure 4.5. % change in stress and strain range and plastic strain energy compared to the stable hysteresis loop for eutectic Sn-Ag thermal cycling.

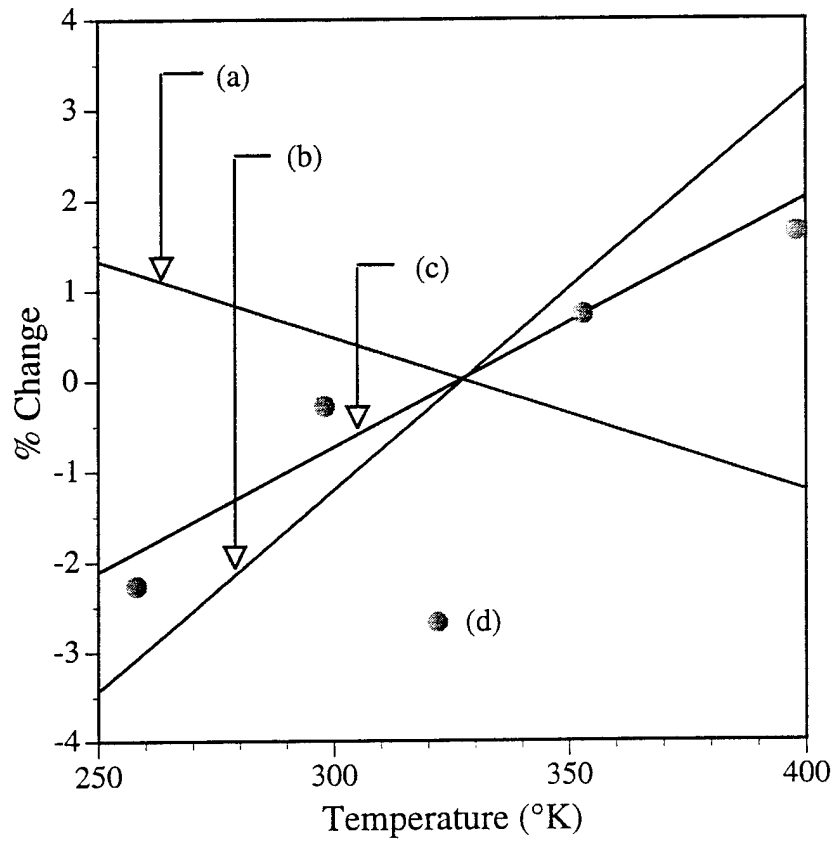
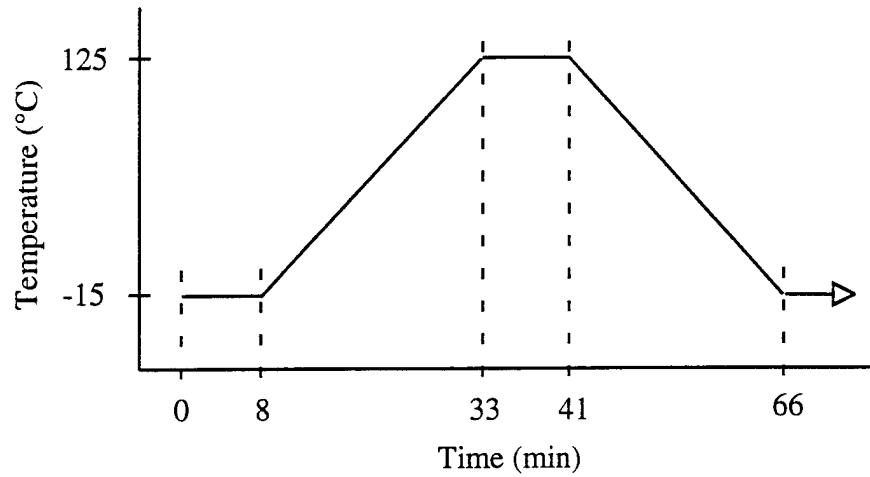
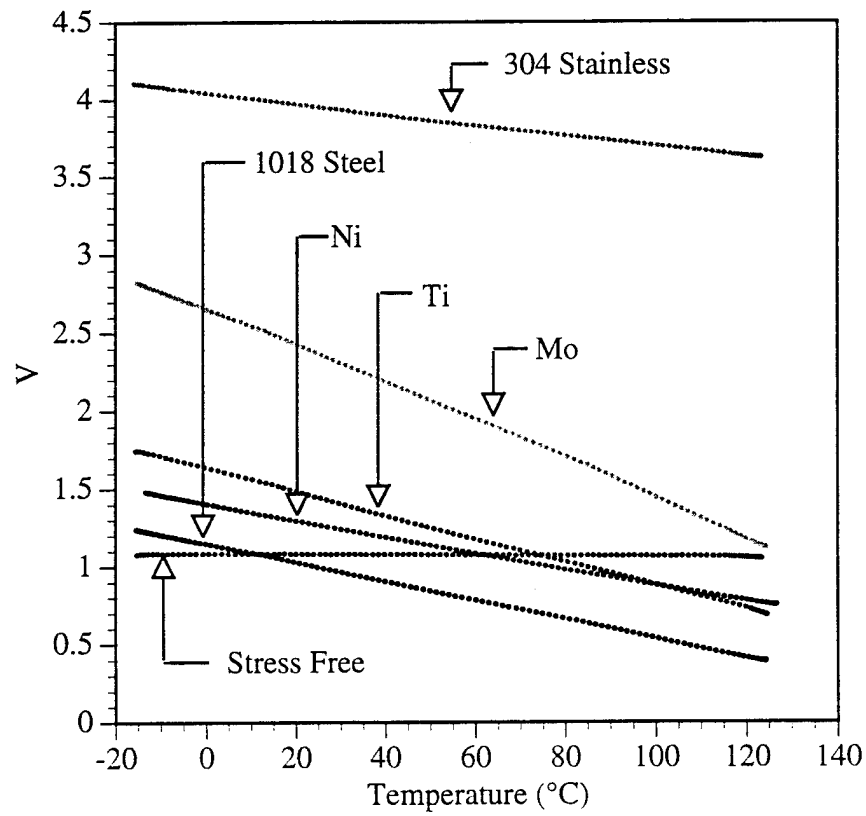


Figure A1.2. a) % change in gage factor, b) expected change in measured strain due to change in elastic modulus of load frame, c) sum of gage and load frame elastic contribution and d) experimentally measured change in dP/dV , all normalized about the median temperature, 55°C .

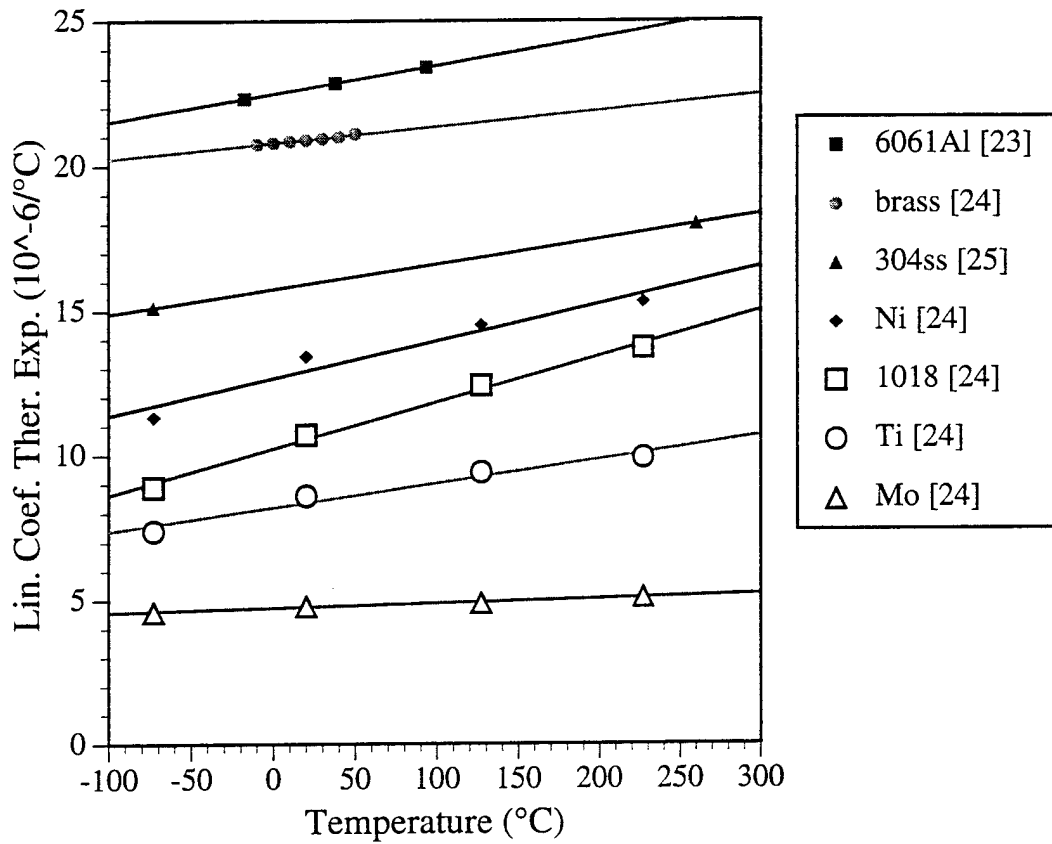


(a)



(b)

Figure A1.3. a) Experimental thermal cycle and b) plot of voltage vs. temperature for each insert pinned with a stainless steel dowel in place of the solder joint.



Al: $\alpha = 9.72E-3 \cdot T + 22.49$
 Brass: $\alpha = 5.61E-3 \cdot T + 20.79$
 304ss: $\alpha = 8.64E-3 \cdot T + 15.75$
 Ni: $\alpha = 1.59E-2 \cdot T + 12.68$ ($10^{-6}/^{\circ}\text{C}$)
 1018: $\alpha = 1.75E-2 \cdot T + 10.24$
 Ti: $\alpha = 9.94E-3 \cdot T + 8.222$
 Mo: $\alpha = 1.49E-3 \cdot T + 4.730$

Figure A1.4. Thermal expansion coefficients and linear fits of the data used to calculate length changes of materials used in the study.

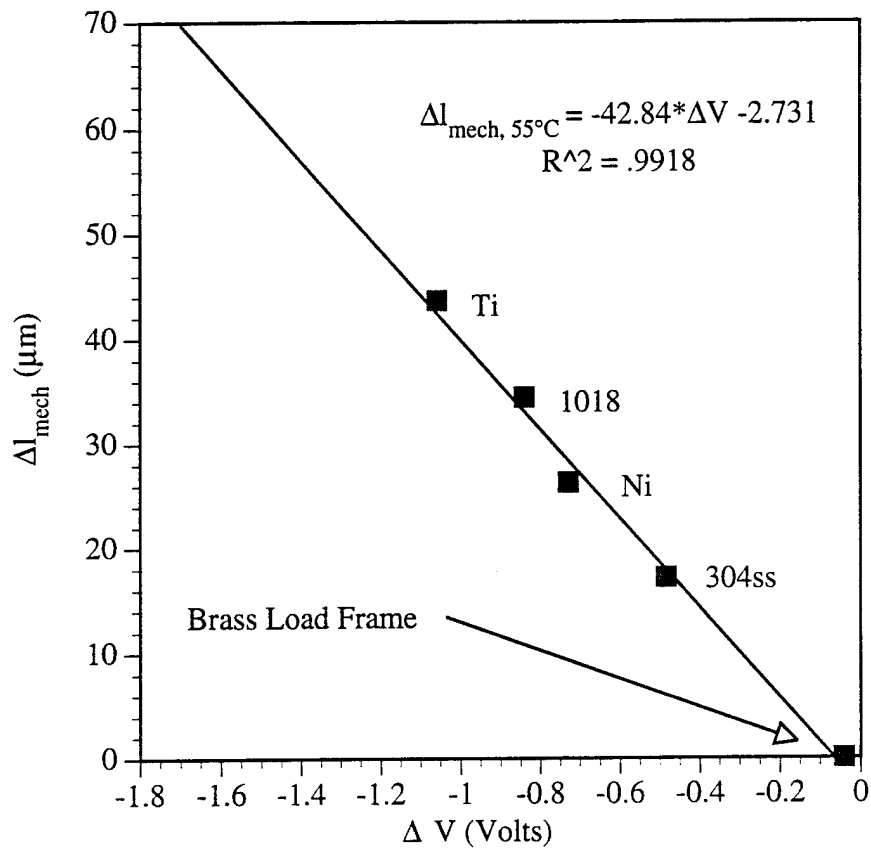


Figure A1.5. Discrete mechanical strains (for various insert materials) and corresponding voltage changes.

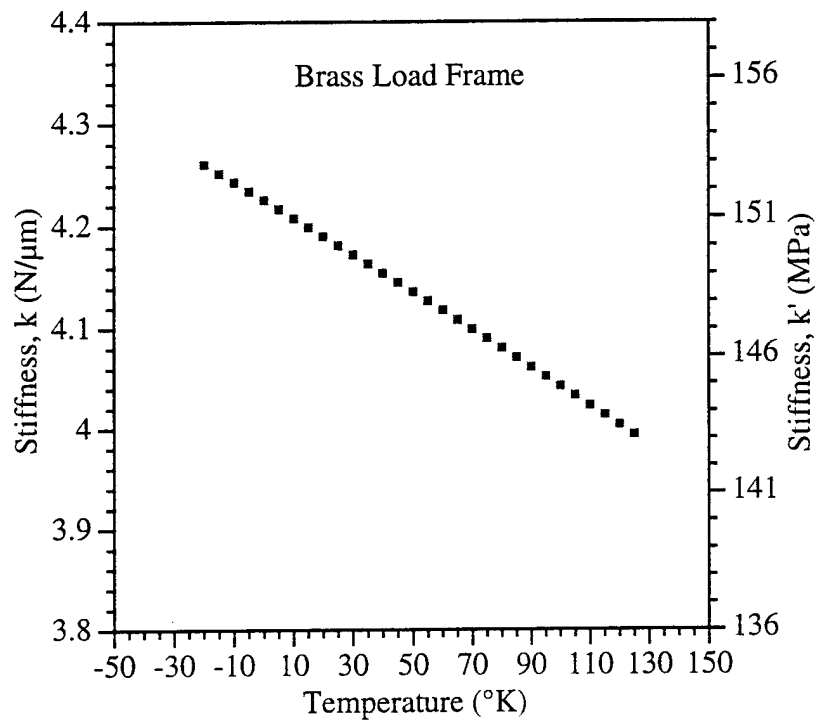


Figure A1.6. Stiffness, k and k' , of brass load frame as a function of temperature.

Appendix 2.
NUMERICAL SIMULATION OF
STABLE THERMOMECHANICAL HYSTERESIS

The stable thermomechanical hysteresis loop can be predicted if the creep properties of the solder are known. Isothermal, tensile creep testing on dog-bone type creep specimens of eutectic Sn-Ag solder has been performed before, and the results are reported in the literature [19]. Steady-state strain rate data were fit to an equation of the form:

$$\dot{\epsilon}_{ss} = \frac{CE}{kT} \left(\frac{\sigma}{E} \right)^n \exp\left(\frac{-Q}{kT} \right) \quad (A2.1)$$

The constant, C, is 4×10^{23} eV/(MPa•sec) and E is given by Equation (A2.2) which gives Young's modulus (MPa) as a function of temperature (°C) [20] as:

$$E = 55.7E3 - 95.4 * T \quad (A2.2)$$

The stress exponent, n, equals 6.7 and the activation energy, Q, is 0.65 eV.

The hysteresis is numerically simulated by incrementally stepping through time and temperature. Following the method of Clech and Augis [21], the stress at any point in a thermal cycle is given by:

$$\tau_{sold} = k' \left(\frac{L}{h} \Delta\alpha(T - T_o) - \gamma_{sold} \right) \quad (A2.3)$$

where all variables are as defined above. T_o is found from the initial stress using Equations (2) and (7) and by using $\Delta l_{sold} = 0.0$ at time equal to zero. Shear stress is then converted to tensile stress for use in Equation (A2.1). Assuming von Mises yielding applies to the creep deformation:

$$\sigma = \sqrt{3} \cdot \tau_{sold} \quad (A2.4)$$

The calculated tensile strain rate is converted to shear strain rate [22] by:

$$\dot{\gamma} = \sqrt{3} \cdot \dot{\epsilon} \quad (A2.5)$$

The shear strain rate is multiplied by the time increment and summed with prior strain. The summed strain, γ_{solid} , is inserted into Equation (A2.3). By incrementally cycling through time and temperature, the stress, strain rate, and creep strain are calculated to generate the thermomechanical hysteresis. The stable simulated hysteresis is compared to the 39th experimentally measured hysteresis loop in Figure A2.1. Stress and strain range are well approximated.

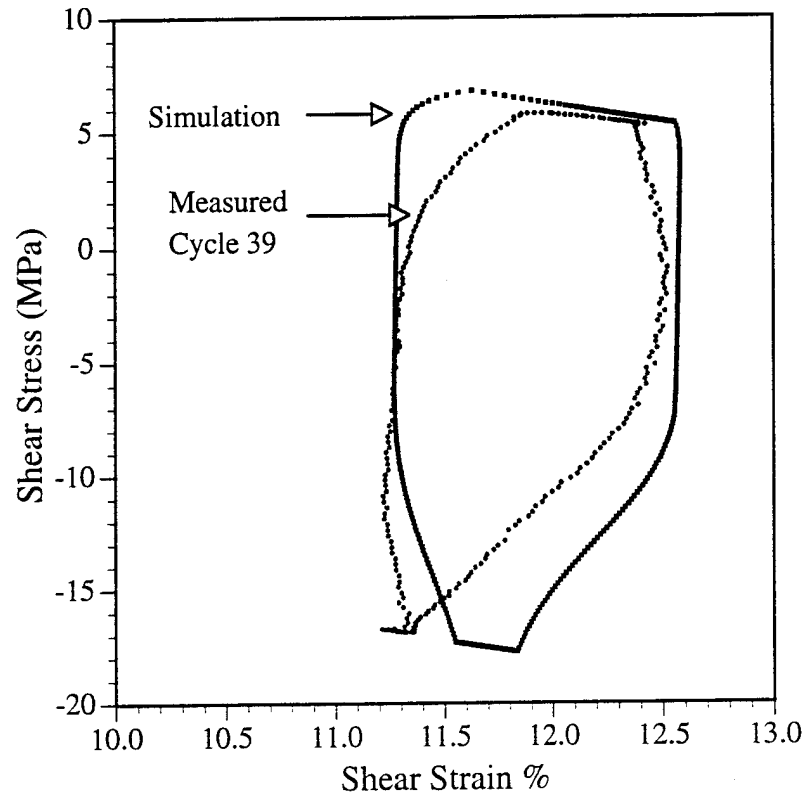


Figure A2.1. Comparison of simulated and experimentally measured stable hysteresis.